

# Model-independent analysis of Airy structures in the $^{16}\text{O} + ^{12}\text{C}$ and $^{16}\text{O} + ^{16}\text{O}$ elastic scattering differential cross sections at 13–22 MeV/nucleon

V. Yu. Korda,<sup>1,\*</sup> A. S. Molev,<sup>1,†</sup> L. P. Korda,<sup>1,2</sup> and V. F. Klepikov<sup>1</sup>

<sup>1</sup>*Institute of Electrophysics and Radiation Technologies, National Academy of Sciences of Ukraine  
28 Chernyshevsky St., P. O. BOX 8812, UA-61002 Kharkov, Ukraine*

<sup>2</sup>*NSC Kharkov Institute of Physics and Technology, National Academy of Sciences of Ukraine  
1 Akademicheskaya St., UA-61108 Kharkov, Ukraine*

(Received 12 November 2008; published 3 February 2009)

We present the results of the model-independent analysis of Airy structures in the  $^{16}\text{O} + ^{12}\text{C}$  and  $^{16}\text{O} + ^{16}\text{O}$  elastic scattering differential cross sections at 13–22 MeV/nucleon. The analysis has been performed with help of a procedure based on the application of the evolutionary algorithm, which enables us to extract the nuclear part of the scattering matrix  $S_N(l)$  as a complex function of angular momentum directly from the scattering data. Contrary to the commonly used model approaches, our procedure gives the better fits and leads to the  $S_N(l)$  representations defined by the moduli and the nuclear phases exhibiting smooth monotonic dependencies on  $l$ .

DOI: [10.1103/PhysRevC.79.024601](https://doi.org/10.1103/PhysRevC.79.024601)

PACS number(s): 24.10.Ht, 25.70.Bc

## I. INTRODUCTION

During the last two decades, the main interest in the study of high-precision data on light nucleus-nucleus elastic scattering at intermediate energies lies in the explanation of the details of complicated rainbow-type refractive structures (Airy structures) observed in the differential cross sections for the elastic scattering of  $^{16}\text{O}$  nuclei by light nuclei at  $E \geq 10$ –15 MeV/nucleon (see, e.g., Refs. [1–3]). These structures manifest themselves particularly as deep Airy minima of the first and higher orders, which are the most pronounced for the  $^{16}\text{O} + ^{12}\text{C}$  system at  $E = 200$  MeV and for the  $^{16}\text{O} + ^{16}\text{O}$  system at  $E = 350$  MeV [4–6]. The results of theoretical analysis of these structures point to the possibility of probing the internal region of the nucleus-nucleus interaction and gaining new valuable information about this interaction. Quantitative description of the refractive behavior of the cross section at large scattering angles, alongside with the damping diffraction oscillations, is important for the unambiguous extraction of the scattering matrix (optical potential) from the data.

The results of the up-to-date calculations based on both the  $S$ -matrix and the optical model formalisms (see, e.g., Refs. [5,7–9]) show that good description of the measured elastic scattering differential cross sections for the  $^{16}\text{O} + ^{12}\text{C}$  and  $^{16}\text{O} + ^{16}\text{O}$  systems is achieved with the help of the nuclear part of the scattering matrix (in the angular momentum space)  $S_N(l) = \eta(l) \exp[2i\delta_r(l)]$ , in which the modulus  $\eta(l) = \exp[-2\delta_a(l)]$  [the nuclear absorption phase  $\delta_a(l)$ ] and the nuclear refraction phase  $\delta_r(l)$  are not smooth monotonic functions of  $l$ . Moreover, different theoretical models lead to different nonmonotonic structures (including the structures having nonsmooth behavior) in moduli  $\eta(l)$  and phases  $\delta_r(l)$ . One may wish to reveal how much the mentioned nonmonotonic structures are physically reasonable and have

well-tested forms. Clearly, only when the same nonmonotonic structures appear in  $\eta(l)$  [ $\delta_r(l)$ ] each time as the result of application of different fitting procedures, one must admit their existence and give them proper physical interpretation.

In the context, it seems valuable to study the possibility of replication of the data in question via the scattering matrix approach with smooth monotonic dependencies of the modulus  $\eta(l)$  and the phase  $\delta_r(l)$  on the angular momentum  $l$ . To achieve this goal, we use the model-independent  $S$ -matrix approach [10] based on the application of the smooth evolutionary algorithm, which is able to extract the nuclear part of the scattering matrix as a complex function of  $l$  directly from the experimental data on the nucleus-nucleus elastic scattering differential cross sections at intermediate energies.

In this publication, we present the results of the analysis of the differential cross sections for  $^{16}\text{O}$ - $^{12}\text{C}$  elastic scattering at  $E = 13$  and 19 MeV/nucleon and for  $^{16}\text{O}$ - $^{16}\text{O}$  elastic scattering at  $E = 16$  and 22 MeV/nucleon, obtained with the help of the model-independent approach [10]. Note that the analysis performed covers the mentioned cross sections with the most clearly pronounced Airy minima among all studied  $^{16}\text{O}$ -nucleus elastic scattering differential cross sections at  $E \geq 13$  MeV/nucleon.

## II. RESULTS OF CALCULATIONS AND THEIR DISCUSSION

Figures 1–5 show the results of application of the model-independent approach we use (details are in Refs. [10,13]). For each of the studied nuclear systems at the given energy, we have extracted the nuclear part of the scattering matrix  $S_N(l)$  defined by the phases  $\delta_a(l)$  [the modulus  $\eta(l)$ ] and  $\delta_r(l)$  which are smooth monotonic functions of  $l$  due to the automatic control of the behavior of the first few derivatives of the phases  $\delta_a(l)$  and  $\delta_r(l)$ . At the same time, the quantum deflection function, which is  $\Theta(l) = 2d[\delta_r(l) + \sigma_C(l)]/dl$  where  $\sigma_C(l)$  is

\*Corresponding author: [kvyu@kipt.kharkov.ua](mailto:kvyu@kipt.kharkov.ua)

†[mas@kipt.kharkov.ua](mailto:mas@kipt.kharkov.ua)

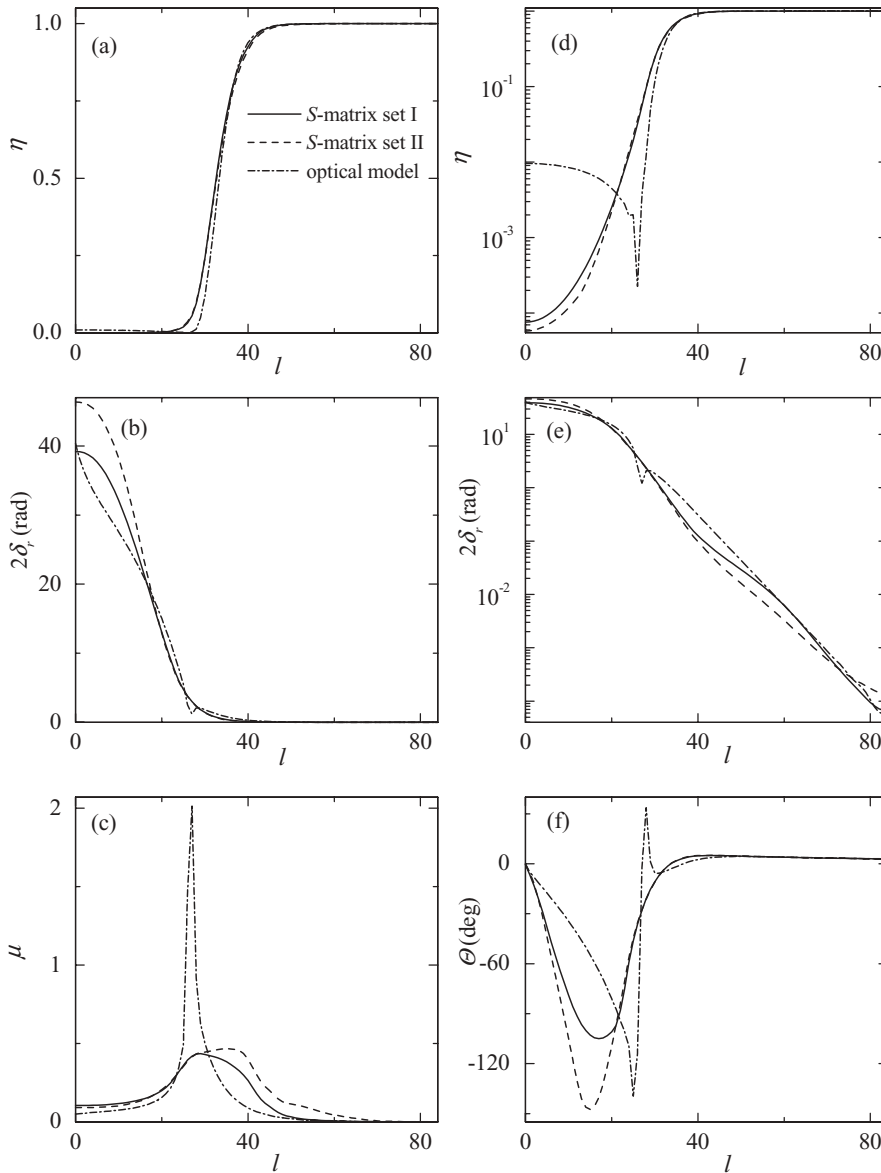


FIG. 1. Two scattering matrices (sets I and II) for the  $^{16}\text{O}$ - $^{12}\text{C}$  elastic scattering at 200 MeV, which give similar fits, together with the one obtained from the optical potential of Ref. [4]. (a) Scattering matrix moduli  $\eta(l)$ . (b) Nuclear phases  $\delta_r(l)$ . (c) Reduced imaginary scattering phases  $\mu(l)$ . (d) Same as (a), but in the logarithmic scale. (e) Same as (b), but in the logarithmic scale. (f) Deflection functions  $\Theta(l)$ .

the Coulomb scattering phase, is typical of the case of a nuclear rainbow. The behavior of the “reduced” imaginary scattering phase  $\mu(l) = \delta_a(l)/\delta_r(l)$  testifies to the fact that the scattering matrix belongs to the systematics described in Refs. [6,14]: the quantity  $\mu(l)$  acquires small values where the angular momenta are small (due to the noticeable transparency of the nucleus with respect to the waves with small angular momenta), has maximum (the value of which is usually about the unity) in the vicinity of the strong absorption momentum, and demonstrates rapid and smooth fall-off at large  $l$ .

The extracted characteristics  $\eta(l)$ ,  $\delta_r(l)$ ,  $\mu(l)$ , and  $\Theta(l)$  are displayed in Figs. 1–4. For the  $^{16}\text{O}$ - $^{12}\text{C}$  scattering, as well as for the  $^{16}\text{O}$ - $^{16}\text{O}$  scattering, at each energy considered we have found two different sets for the  $S_N(l)$  dependencies (sets I and II in Figs. 1–4). The values of the nuclear rainbow angle  $\theta_R$  [which corresponds to the minimum of the deflection function  $\Theta(l)$ ], the total reaction cross section  $\sigma_R^t$  and  $\chi^2/N$  ( $N$  is the number of experimental points) for the calculated cross

sections are presented in Table I. The values of  $\mu(0)$  for both sets of the  $S$ -matrix representation at the energies under study are not larger than 0.15.

TABLE I. Obtained nuclear rainbow angles  $\theta_R$ , total reaction cross sections  $\sigma_R^t$ , and  $\chi^2/N$  values.

System	$E$ (MeV)	$S$ -matrix set	$\theta_R$ (deg)	$\sigma_R^t$ (mb)	$\chi^2/N$
$^{16}\text{O} + ^{12}\text{C}$	200.0	I	105	1473	3.1
		II	148	1500	3.0
	300.0	I	58	1392	1.9
		II	94	1397	2.0
$^{16}\text{O} + ^{16}\text{O}$	250.0	I	93	1743	2.6
		II	139	1746	3.1
	350.0	I	64	1689	2.9
		II	101	1664	3.0

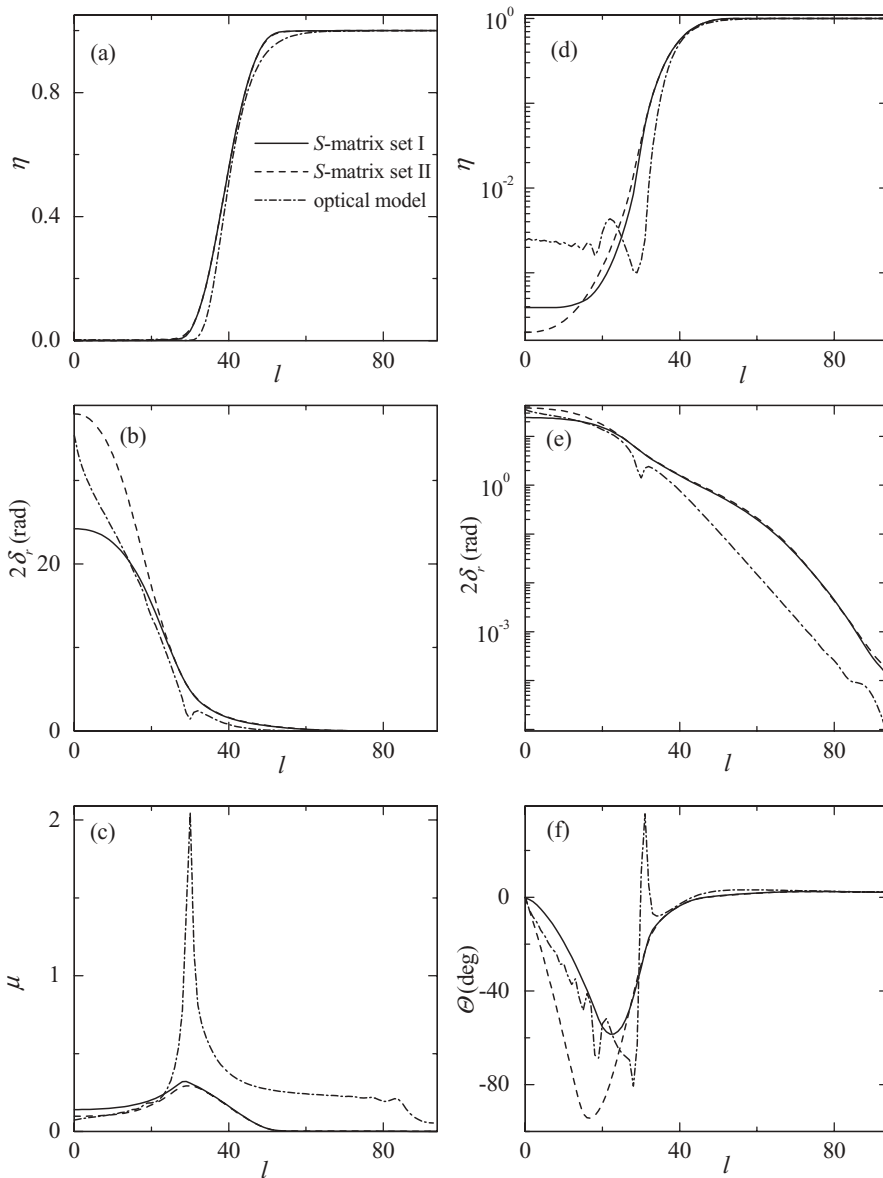


FIG. 2. Same as Fig. 1, but for the  $^{16}\text{O}-^{12}\text{C}$  elastic scattering at 300 MeV. Dash-dotted curves show the results of the calculations with the use of the optical potential [11].

The corresponding differential cross sections are shown in Fig. 5. We see that in each case under investigation, the data are correctly described by the calculated differential cross section in the whole angular range considered. The cross sections were fitted assuming the 10% error bars (see, e.g., Refs. [2,4,10]). Because of the limited angular range where the data were measured, we have supplemented the existing set of data with several additional pseudo data points lying outside this limited range in order to demonstrate the behavior of the cross section at larger scattering angles (see Refs. [10,15]). This procedure forces the calculated differential cross section to have the prescribed behavior up to the angles  $\theta \approx 140^\circ$  and  $100^\circ$  for the  $^{16}\text{O}-^{12}\text{C}$  scattering at  $E = 200$  and  $300$  MeV, respectively, and up to  $\theta \approx 80^\circ$  for the  $^{16}\text{O}-^{16}\text{O}$  scattering at  $350$  MeV. Note that the mentioned procedure is not always justified and should be applied with care, paying attention to the features of the behavior of the studied differential cross sections at large angles. The analysis of the differential cross sections in the

extended angular range is performed only after the fitting to the actual set of measured data has been completed.

For the comparison with our results, Figs. 1–4 also contain the curves for  $\eta(l)$ ,  $\delta_r(l)$ ,  $\mu(l)$ , and  $\Theta(l)$  calculated with help of the six- and nine-parameter model representations of the optical potential, which provide very satisfactory fits to the data. As we see, the moduli  $\eta(l)$  and phases  $\delta_r(l)$  contain separate nonmonotonic structures. At the same time, the quality of fits to the data under study with the use of these values is worse than that achieved by us. The behavior of  $S_N(l)$  for the considered cases of the  $^{16}\text{O} + ^{12}\text{C}$  and  $^{16}\text{O} + ^{16}\text{O}$  scattering, obtained within the  $S$ -matrix approaches [7,16,17] substantially differs from that found by us, due to the existence of the nonmonotonic structures in  $\eta(l)$  and  $\Theta(l)$  [ $\delta_r(l)$ ] associated with the manifestation of the separate Regge poles. The application of these  $S_N(l)$  in all considered cases, except for the results of Ref. [7], leads to noticeably worse agreement between the calculated cross sections and

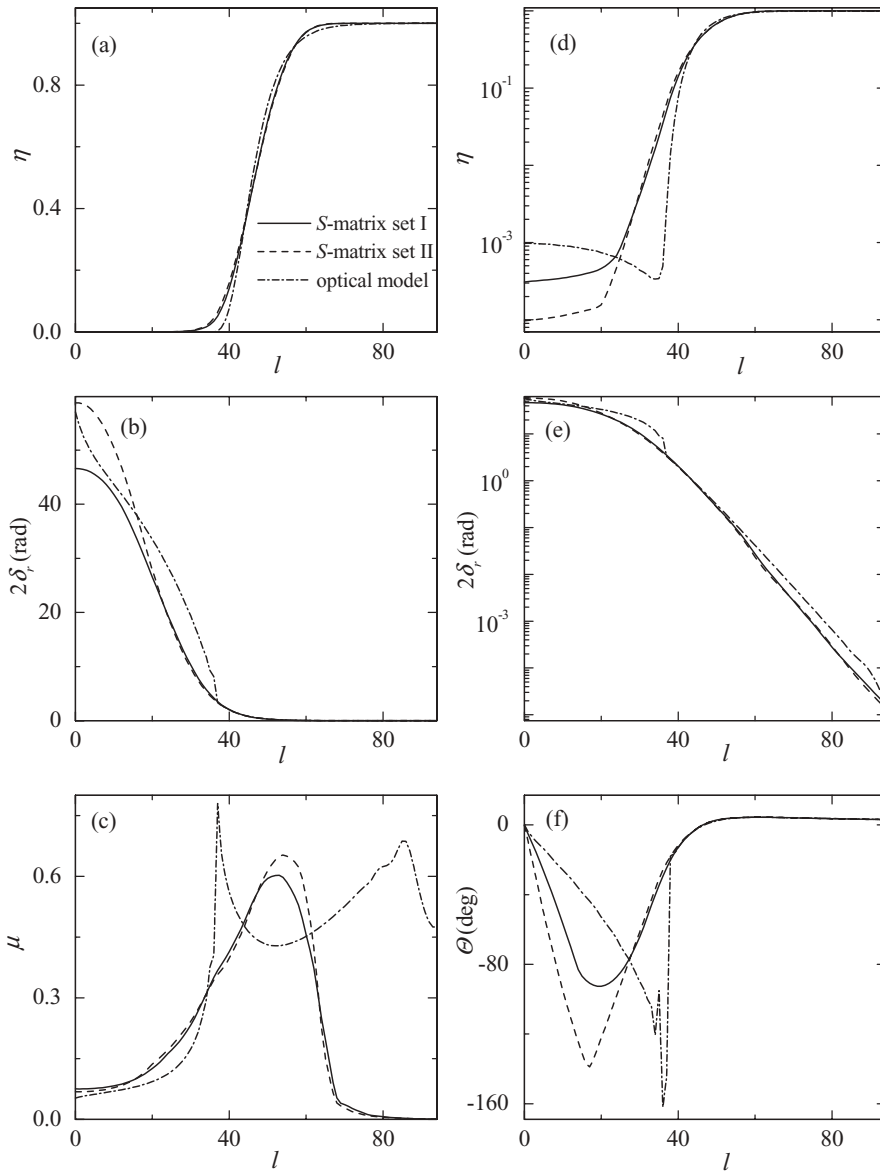


FIG. 3. Same as Fig. 1, but for the  $^{16}\text{O}$ - $^{16}\text{O}$  elastic scattering at 250 MeV. Dash-dotted curves show the results of the calculations with the use of the optical potential [2].

the experimental data, as compared to our results presented in Fig. 5.

Within the model-independent  $S$ -matrix approach used, further improvement of the quality of fit, keeping the smooth and monotonic behavior of the modulus  $\eta(l)$  and the nuclear phase  $\delta_r(l)$ , can be achieved if we abandon some requirements imposed on the shapes of  $\delta_{a,r}(l)$  (see, Ref. [10]). For instance, if we do not control the third derivative of  $\delta_r(l)$  and, sometimes, the second derivative of  $\delta_a(l)$ , then the values of  $\chi^2/N$  can be reduced by 10–30%. If we abandon all the imposed requirements, then we permit the appearance of the nonmonotonic structures in  $\eta(l)$  and  $\delta_r(l)$  and become able to obtain much better quality of fit in all the cases studied and, particularly, for the  $^{16}\text{O}$ - $^{16}\text{O}$  scattering at  $E = 350$  MeV, where it turns out to be not worse than that found in Refs. [7,8]. However, the nonmonotonic structures that arise in  $\eta(l)$  and  $\delta_r(l)$  in this case appear quite different from run to run of the fitting procedure and from the structures found

in Refs. [7,8]. Taking into account these observations, one cannot justify the existence of the mentioned nonmonotonic structures.

Analyzing the behavior of  $\eta(l)$ ,  $\delta_r(l)$ ,  $\Theta(l)$  (Figs. 1–4), we see that set II is characterized by stronger absorption and nuclear refraction in the region of small angular momenta as compared to these values for set I, so there appear the change of the nuclear rainbow angle to larger values and the shift of the primary rainbow maximum (and the preceding minimum, if any) to larger angles. This leads us to the idea that the pronounced maximum around  $90^\circ$  in the  $^{16}\text{O}$ - $^{12}\text{C}$  scattering cross section at  $E = 200$  MeV and the broad maxima around  $50^\circ$  in the cross sections for the  $^{16}\text{O} + ^{12}\text{C}$  system at  $E = 300$  MeV and for the  $^{16}\text{O} + ^{16}\text{O}$  system at  $E = 350$  MeV should be interpreted as the primary rainbow maxima for set I and as the secondary rainbow maxima for set II. The deep minimum around  $66^\circ$  in the cross section for the  $^{16}\text{O}$ - $^{12}\text{C}$  scattering at  $E = 200$  MeV as well as the minima around  $45^\circ$  and  $44^\circ$  in

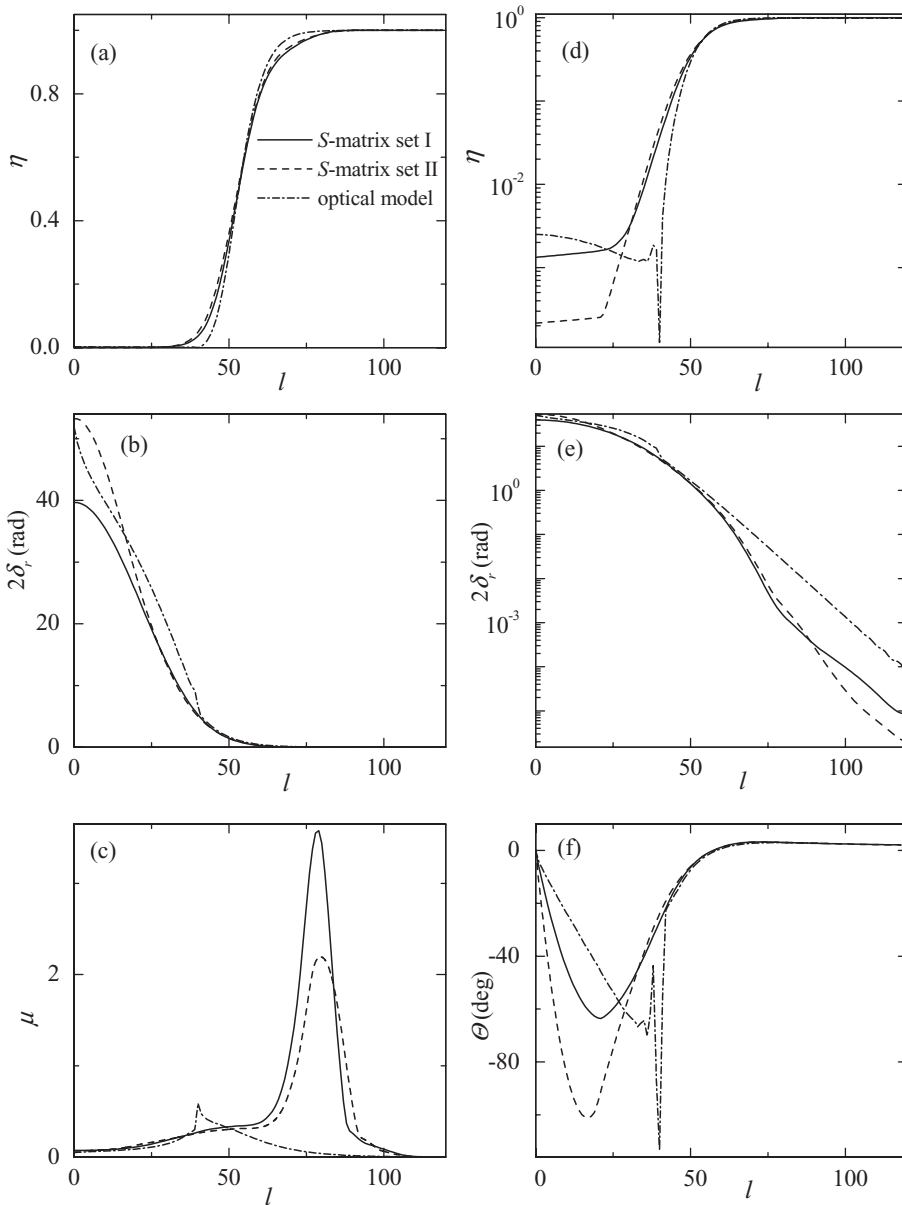


FIG. 4. Same as Fig. 1, but for the  $^{16}\text{O}$ - $^{16}\text{O}$  elastic scattering at 350 MeV. Dash-dotted curves show the results of the calculations with the use of the optical potential [5].

the cross sections for the  $^{16}\text{O}$ - $^{12}\text{C}$  scattering at  $E = 300$  MeV and the  $^{16}\text{O}$ - $^{16}\text{O}$  scattering at  $E = 350$  MeV, respectively, are the first-order Airy minima for set I and the second-order Airy minima for set II. At  $E = 250$  MeV, the refractive structures in the  $^{16}\text{O}$ - $^{16}\text{O}$  scattering cross section appear less pronounced than at  $E = 350$  MeV. Particularly at  $\theta \geq 80^\circ$ , the Airy structure, including the rainbow maximum, is masked by the interference oscillations conditioned by the symmetrization of the scattering amplitude in the case of scattering of identical nuclei.

Note the coincidence of our results of the identification of Airy structures in the  $^{16}\text{O}$ - $^{12}\text{C}$  elastic scattering differential cross sections with those obtained in Refs. [4,18] where two different families of the optical Woods-Saxon potentials (strongly different by the depths of the real parts) have been extracted from the data. The presented identification of the

rainbow features in the  $^{16}\text{O}$ - $^{16}\text{O}$  scattering cross section at  $E = 350$  MeV is the same as in Refs. [2,5,19].

More detailed analysis of refractive and diffractive features of the structures appearing in the elastic scattering cross sections under discussion at midangles and large angles can be performed with the use of the nearside/farside decomposition [20]. Concerning the deep minimum around  $66^\circ$  in the cross section for the  $^{16}\text{O}$ - $^{12}\text{C}$  scattering at  $E = 200$  MeV, we emphasize that it is dominated by the farside amplitude (see Fig. 6). However, the influence of the nearside amplitude persists, and the interference effects between farside and nearside amplitudes are present. Although the formation of the considered minimum occurs under the conditions of predominant influence of nuclear refraction, the features of this minimum are determined by specific combination of the values of nuclear refraction, absorption, and Coulomb

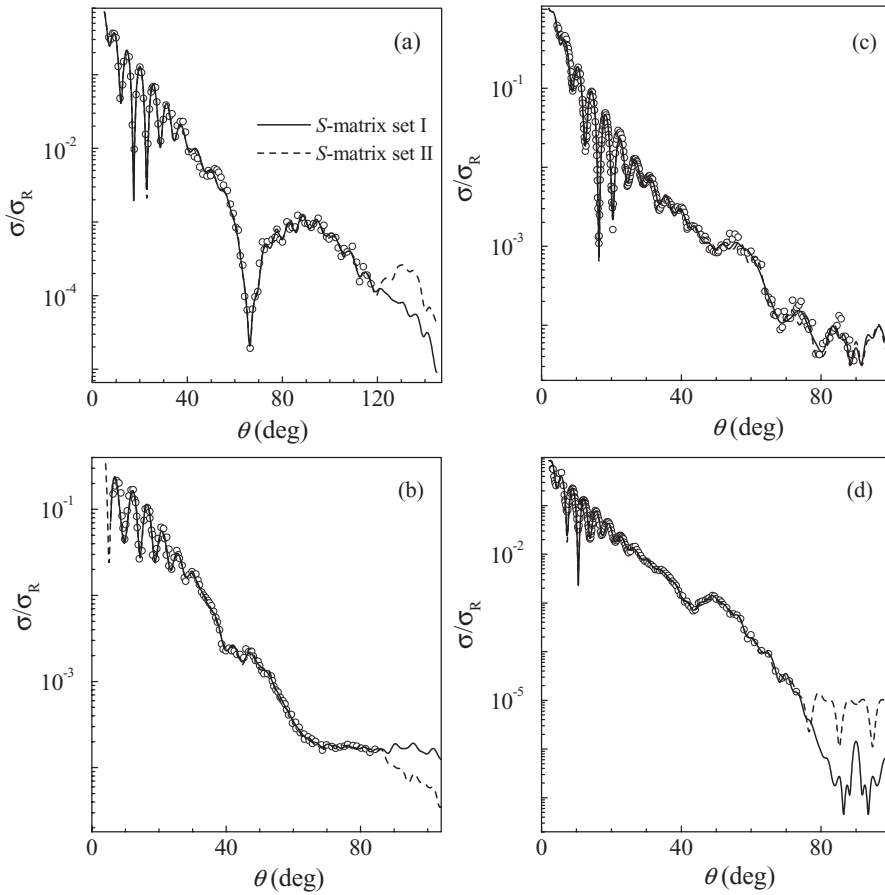


FIG. 5. Elastic scattering differential cross sections calculated using the *S*-matrix sets I and II. (a)  $^{16}\text{O} + ^{12}\text{C}$  system at 200 MeV. (b)  $^{16}\text{O} + ^{12}\text{C}$  system at 300 MeV. (c)  $^{16}\text{O} + ^{16}\text{O}$  system at 250 MeV. (d)  $^{16}\text{O} + ^{16}\text{O}$  system at 350 MeV. The data are from Refs. [2,4,5,11,12].

interaction. All important details of other cross sections under consideration at angles  $\theta \geq 40^\circ$ , including the minimum at  $44^\circ$  (followed by a broad rainbow maximum) observed in the  $^{16}\text{O} + ^{16}\text{O}$  data at 350 MeV and the structure around  $70^\circ$  in the  $^{16}\text{O} + ^{12}\text{C}$  cross section at 300 MeV, are fully reproduced by the farside contributions, as was already discussed in Refs. [2,18]. Thus, the interpretation of these details in terms

of the considered approach is the same as presented in the mentioned papers.

Figure 5 shows that the existence of the experimental data in the angular range  $\theta \geq 120^\circ$  for the  $^{16}\text{O}-^{12}\text{C}$  scattering at  $E = 200$  MeV, and  $\theta \geq 75^\circ$  and  $85^\circ$  for the  $^{16}\text{O}-^{16}\text{O}$  scattering at  $E = 350$  MeV, and the  $^{16}\text{O}-^{12}\text{C}$  scattering at  $E = 300$  MeV, respectively, would make the analysis more unambiguous.

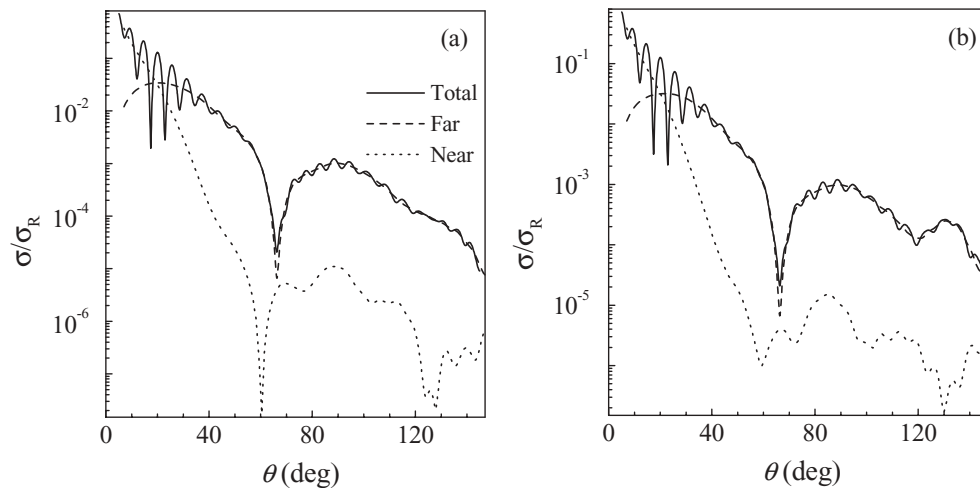


FIG. 6. Nearside/farside decomposition of the  $^{16}\text{O}-^{12}\text{C}$  cross sections at 200 MeV performed using the *S*-matrix sets I (a) and II (b).

### III. CONCLUSION

The analysis of the elastic scattering differential cross sections for the systems  $^{16}\text{O} + ^{12}\text{C}$  and  $^{16}\text{O} + ^{16}\text{O}$  at the bombarding energies  $E = 13\text{--}22$  MeV/nucleon, performed on the basis of the model-independent  $S$ -matrix approach [10], has enabled us to get quantitative description of the existing data and to identify the rainbow maxima and the Airy minima of the first and higher orders. To unambiguously interpret the pronounced Airy structures in the considered cross sections for the elastic  $^{16}\text{O} + ^{12}\text{C}$  and  $^{16}\text{O} + ^{16}\text{O}$  scattering, one needs to perform the analysis of the data measured in the wider angular range.

We point out that in all studied cases of the nucleus-nucleus scattering, the modulus  $\eta(l)$  and the nuclear phase  $\delta_r(l)$ , which determine the nuclear part of the scattering matrix, are smooth monotonic functions of the angular momentum, while the

quantum deflection function  $\Theta(l)$  has a form characteristic of the nuclear rainbow case. The reduced imaginary scattering phase  $\mu(l)$  belongs to the systematics considered in Refs. [6,14].

The results of the performed analysis clearly testify to the fact that the existence of the separate nonmonotonic structures (including the structures having nonsmooth behavior) in  $\eta(l)$  and  $\delta_r(l)$  [ $\Theta(l)$ ] for the systems  $^{16}\text{O} + ^{12}\text{C}$  and  $^{16}\text{O} + ^{16}\text{O}$  at the energies under consideration is not justified.

### ACKNOWLEDGMENTS

We are indebted to Dao T. Khoa for providing us with the experimental data for the  $^{16}\text{O} + ^{16}\text{O}$  system in tabulated form.

- 
- [1] M. E. Brandan and G. R. Satchler, *Phys. Rep.* **285**, 143 (1997).  
 [2] D. T. Khoa, W. von Oertzen, H. G. Bohlen, and F. Nuoffer, *Nucl. Phys.* **A672**, 387 (2000).  
 [3] D. T. Khoa, W. von Oertzen, H. G. Bohlen, and S. Ohkubo, *J. Phys. G* **34**, R111 (2007).  
 [4] A. A. Ogloblin, Yu. A. Glukhov, V. Trzaska, A. S. Dem'yanova, S. A. Goncharov, R. Julin, S. V. Klebnikov, M. Mutterer, M. V. Rozhkov, V. P. Rudakov, G. P. Tiorin, D. T. Khoa, and G. R. Satchler, *Phys. Rev. C* **62**, 044601 (2000).  
 [5] M. E. Brandan and G. R. Satchler, *Phys. Lett.* **B256**, 311 (1991).  
 [6] M. E. Brandan and K. W. McVoy, *Phys. Rev. C* **55**, 1362 (1997).  
 [7] L. J. Allen, L. Berge, C. Steward, K. Amos, H. Fiedeldey, H. Leeb, R. Lipperheide, and P. Fröbrich, *Phys. Lett.* **B298**, 36 (1993).  
 [8] S. G. Cooper and R. S. Mackintosh, *Nucl. Phys.* **A576**, 308 (1994).  
 [9] G. Bartnitzky, A. Blazevic, H. G. Bohlen, J. M. Casandjian, M. Chartier, H. Clement, B. Gebauer, A. Gillibert, Th. Kirchner, D. T. Khoa, A. Lepine-Szily, W. Mittig, W. von Oertzen, A. N. Ostrowski, P. Roussel-Chomaz, J. Siegler, M. Wilpert, and Th. Wilpert, *Phys. Lett.* **B365**, 23 (1996).  
 [10] V. Yu. Korda, A. S. Molev, and L. P. Korda, *Phys. Rev. C* **72**, 014611 (2005).  
 [11] M. E. Brandan, A. Menchaca-Rocha, L. Trache, H. L. Clark, A. Azhari, C. A. Gagliardi, Y.-W. Lui, R. E. Tribble, R. L. Varner, J. R. Beene, and G. R. Satchler, *Nucl. Phys.* **A688**, 659 (2001).  
 [12] E. Stiliaris, H. G. Bohlen, P. Fröbrich, B. Gebauer, D. Kolbert, W. von Oertzen, M. Wilpert, and Th. Wilpert, *Phys. Lett.* **B223**, 291 (1989).  
 [13] V. Yu. Korda, A. S. Molev, and L. P. Korda, *Izv. Ross. Akad. Nauk, Ser. Fiz.* **69**, 1593 (2005).  
 [14] Y. J. Kim and M. H. Cha, *Int. J. Mod. Phys. E* **11**, 211 (2002).  
 [15] M. A. McEwan, S. G. Cooper, and R. S. Mackintosh, *Nucl. Phys.* **A552**, 401 (1993).  
 [16] A. V. Kuznichenko, V. V. Pilipenko, G. M. Onyshchenko, and A. S. Dem'yanova, *Izv. Ross. Akad. Nauk, Ser. Fiz.* **66**, 701 (2002).  
 [17] A. V. Kuznichenko, V. V. Pilipenko, G. M. Onyshchenko, A. S. Dem'yanova, and N. Burtebaev, *Izv. Ross. Akad. Nauk, Ser. Fiz.* **67**, 704 (2003).  
 [18] A. A. Ogloblin, S. A. Goncharov, Yu. A. Glukhov, A. S. Dem'yanova, M. V. Rozhkov, V. P. Rudakov, and W. H. Trzaska, *Phys. At. Nucl.* **66**, 1478 (2003).  
 [19] Y. Kondo, F. Michel, and G. Reidemeister, *Phys. Lett.* **B242**, 340 (1990).  
 [20] R. C. Fuller, *Phys. Rev. C* **12**, 1561 (1975).